



**HAL**  
open science

**Preparation and optical characteristics of novel  
oxynitride phases in the  $R_3(\text{Ta/Nb})\text{-O-N}$  system ( $R =$   
**La, Eu, Gd, Ho, Y, Yb**)**

Erwan Ray, Franck Tessier, François Cheviré

► **To cite this version:**

Erwan Ray, Franck Tessier, François Cheviré. Preparation and optical characteristics of novel oxynitride phases in the  $R_3(\text{Ta/Nb})\text{-O-N}$  system ( $R = \text{La, Eu, Gd, Ho, Y, Yb}$ ). *Solid State Sciences*, 2011, 13 (5), pp.1031-1035. 10.1016/j.solidstatesciences.2011.01.025 . hal-00719428

**HAL Id: hal-00719428**

**<https://hal.science/hal-00719428>**

Submitted on 16 Feb 2016

**HAL** is a multi-disciplinary open access archive for the deposit and dissemination of scientific research documents, whether they are published or not. The documents may come from teaching and research institutions in France or abroad, or from public or private research centers.

L'archive ouverte pluridisciplinaire **HAL**, est destinée au dépôt et à la diffusion de documents scientifiques de niveau recherche, publiés ou non, émanant des établissements d'enseignement et de recherche français ou étrangers, des laboratoires publics ou privés.

# **Preparation and optical characteristics of novel oxynitride phases in the $R_3(\text{Ta/Nb})\text{-O-N}$ system ( $R = \text{La, Eu, Gd, Ho, Y, Yb}$ ).**

Erwan Ray\*, Franck Tessier, François Cheviré

UMR CNRS 6226 "Sciences Chimiques de Rennes", Equipe "Verres et Céramiques",  
Université de Rennes 1, F-35042 Rennes cedex, France

\* Phone: +33 2 23 23 62 56, Fax: +33 2 23 23 56 83, Erwan.Ray@univ-rennes1.fr

## **Keywords**

Rare earth tantalates/niobates, oxynitrides, optical properties, solid solution

## **Abstract**

The synthesis of reactive nitridation precursors prepared by the citrate route has been evidenced with the  $R_3\text{TaO}_7$  and  $R_3\text{NbO}_7$  stoichiometries ( $R = \text{La, Eu, Gd, Ho, Y, Yb}$ ). Novel oxynitride phases have been isolated in the fluorite-type series  $R_3\text{Ta}(\text{O,N},\square)_8$  and  $R_3\text{Nb}(\text{O,N},\square)_8$  where  $\square$  represents anionic vacancies. The niobium/tantalum substitution leads to a modification of the absorption properties towards higher wavelengths. The comparison between  $\text{GdTa}$ ,  $\text{Gd}_2\text{Ta}$  and  $\text{Gd}_3\text{Ta}$ -based oxynitride phases highlights a blue shift of the position of the absorption edge with increasing  $\text{Gd/Ta}$  ratio. Unlike with  $\text{RTa}$  and  $\text{R}_2\text{Ta}$  stoichiometries,  $\text{R}_3\text{Ta}$ - oxynitride phases generally show a very narrow formation range in temperatures as well as low absorption in the visible.

## 1. Introduction

Oxynitride phases belonging to the R-Ta-O-N system were recently studied with the RTa and R<sub>2</sub>Ta stoichiometries [1-2]. Reactions between rare-earth tantalates RTaO<sub>4</sub> and ammonia flow at 950°C form oxynitrides with different structures depending on the size of the R element: perovskite RTaON<sub>2</sub>, pyrochlore R<sub>2</sub>Ta<sub>2</sub>O<sub>5</sub>N<sub>2</sub> (R = Nd to Gd) and defect fluorite RTa(O,N,□)<sub>4</sub> for R = [Ho, Er, Yb, Y] (□ represents an anionic vacancy) [1]. The RTa-O-N oxynitrides with fluorite structure form solid solution domains with variable nitrogen contents and related colors. The color of the YTa(O,N,□)<sub>4</sub> powders varies from yellow (after 15h nitridation) to brown for the most substituted compositions (after 90h). Fluorite-type phases have been also evidenced in the oxynitride series R<sub>2</sub>Ta(O,N,□)<sub>6</sub> with R = [Nd to Yb, Y]. Gd<sub>2</sub>Ta(O,N,□)<sub>6</sub> manifests a bright yellow hue characterized by the CIE color coordinates L = 95, a\* = 2 and b\* = 19 [2].

In the present study, we have pursued our investigations with the exploration of the R<sub>3</sub>Ta stoichiometry. Our interest focused particularly on the gadolinium phase in order to compare its optical characteristics with the previously obtained results in the GdTa-O-N and Gd<sub>2</sub>Ta-O-N stoichiometries [1, 2]. We have also studied the analog compositions by fully substituting niobium for tantalum atoms. Few papers have been devoted to the preparation of R<sub>3</sub>TaO<sub>7</sub> and R<sub>3</sub>NbO<sub>7</sub> ternary oxides. Reports on the crystal structure of R<sub>3</sub>TaO<sub>7</sub> are often confused. Indeed, Yokogawa *et al.* have reported that R<sub>3</sub>TaO<sub>7</sub> compounds showed several polymorphic modifications based on fluorite-related structures [3]. Generally, it is accepted that the decrease in the R<sup>3+</sup> ionic radii leads to a crystal structure of higher symmetry characterized by disordered distributions of cations or anions. The crystal structure of the compounds shifts respectively from

orthorhombic weberite to pyrochlore, and then to defect fluorite from R = La to Yb [4, 5].  $\text{La}_3\text{TaO}_7$  and  $\text{La}_3\text{NbO}_7$  samples prepared by a polymerized complex method are metastable and show a phase transition occurring around 1050 and 1000°C respectively, from cubic pyrochlore to orthorhombic weberite [6, 7]. Similar structure-types were evidenced with  $\text{R}_3\text{NbO}_7$  compositions [8].

The incorporation of nitrogen within such oxide systems allows to shift the absorption edge towards visible wavelengths [9]. In particular, our attention focused on the effect of nitrogen on the colors resulting from the nitridation treatment. Nitride and oxynitride materials display interesting optical properties that can be developed, in a non-exhaustive reference list, among pigments, UV absorbers, visible-light-driven photocatalysts [9-13] or phosphors [14, 15]. Among them, nitrogen-doped  $\text{TiO}_2$  is one of the most investigated material to degrade organic molecules in air or water under visible light [16, 17]. However, oxynitrides and nitrides, containing more nitrogen, exhibit promising performances for overall water splitting to produce hydrogen [18-20].

## **2. Experimental**

### *2.1. Preparation*

$\text{R}_3\text{TaO}_7$  tantalates and  $\text{R}_3\text{NbO}_7$  niobates were prepared using the amorphous citrate route involving citric acid as a complexing agent. This calcination method of metal-organic complexes produces ultrafine reactive powders with an excellent chemical homogeneity [10]. Rare-earth oxides ( $\text{Eu}_2\text{O}_3$ ,  $\text{Ho}_2\text{O}_3$ ,  $\text{Yb}_2\text{O}_3$ ) dissolved in concentrated hydrochloric acid (37%, Merck), rare-earth nitrates (for lanthanum, gadolinium, yttrium) dissolved in distilled water, niobium ammonium oxalate (H.C. Starck) and a tantalum oxalate solution (H.C. Starck) in water were used as starting

materials. Citric acid ( $C_6H_8O_7$ , Merck, >99%.) dissolved in a minimum amount of water was added to each solution in the proportion of 1 mol per cation valence, the addition being followed by a 30 min stirring step at 120 °C. Since the complexation of cations by citric acid is improved at  $pH \geq 7$ , the acidic solutions were neutralized by ammonia solution (25%, Merck) [21]. Then the solutions were mixed together and stirred at 150 °C for 20 min to promote chelate formation. The liquid was progressively heated up to 250 °C, leading after 5 h to an expanded black solid residue. This solid was finally ground and calcined at 600 °C in air in an alumina crucible until elimination of carbon. X-ray amorphous powders are generally produced with a high reactivity for nitridation.

Nitridation reactions were carried out in alumina boats placed inside an electric furnace through which ammonia gas flowed with a flow rate of 20 L.h<sup>-1</sup>. The temperature was raised between 700 and 950 °C at a heating rate of 10 °C.min<sup>-1</sup>. Generally, after a 15 h reaction time, the furnace was switched off and the nitrided powders were allowed to cool to room temperature under nitrogen atmosphere.

## 2.2. Characterization

XRD powder patterns were recorded using a Philips PW3710 diffractometer operating with Cu K $\alpha$  radiation ( $\lambda = 1.5418 \text{ \AA}$ ). X'PERT softwares – Data Collector and Graphics, and Identify – were used, respectively, for pattern recording, analysis and phase matching. The lattice parameters were refined using Dicvol04 [22].

Nitrogen and oxygen contents were determined with a LECO<sup>®</sup> TC-600 analyzer using the inert gas fusion method. Nitrogen was measured as N<sub>2</sub> by thermal conductivity and oxygen as CO<sub>2</sub> by infrared detection. The apparatus was calibrated using Leco<sup>®</sup>

standard oxides as well as  $\epsilon$ -TaN as a nitrogen standard [23]. The estimation of the error on the measurement is lower than 5%.

Diffuse reflectance spectra were collected using a Varian Cary 100 Scan spectrometer equipped with the Varian WinUV software and the integrated sphere Labsphere (DRC-CA-30I). Prior to measurements, the absolute reflectance of the samples was calibrated with a certified "spectralon" standard (Labsphere Cie). Experimental data were collected within the 250-800 nm range with 1 nm step and 0.5 s integration time. The position of the absorption edge was determined graphically at the inflexion point of the curve and the value of the optical gap using the theory of Kubelka-Munk [24]. The CIE  $L^*a^*b^*$  color coordinates, L: brightness axis,  $a^*$ : green to red axis,  $b^*$ : blue to yellow axis, were deduced from the diffuse reflectance spectra (Varian software: WinUV Color Application). Energy-dispersive Spectrometry (EDS) has been used to determine the R:(Ta,Nb) ratio of the samples. The EDS analysis system works as an integrated feature of a scanning electron microscope (JEOL JSM 6400).

### **3. Results and Discussion**

#### *3.1. $R_3TaO_7 / R_3NbO_7$ oxide precursors*

Rare-earth tantalates and niobates form a large family of compositions with the stoichiometries  $R(Ta/Nb)O_4$ ,  $R_3(Ta/Nb)O_7$ ,  $R(Ta/Nb)_3O_9$ ,  $R(Ta/Nb)_7O_{19}$ ,  $R_3(Ta/Nb)O_6$  [25]. In this work, our contribution to the system R-Ta-O-N is extended to the nitridation of the  $R_3TaO_7$  compositions (R = La, Eu, Gd, Ho, Y, Yb). Among the possibilities offered by the complexation-calcination method, oxide precursors can be prepared as reactive X-ray amorphous powders. This route often allows to prepare

metastable oxides as reported in the  $Y_6(W,Mo)O_{12}$  solid solution for which a cubic structure is observed at low temperatures instead of the thermodynamically stable rhombohedral one [26]. In the present study, the thermal reaction of amorphous precursors at 1000°C during 15h leads unambiguously to a crystallized fluorite-type phase  $R_3TaO_7$ , as shown for gadolinium in Fig. 1a, except for the lanthanum compound that crystallizes in an orthorhombic weberite structure ( $a = 11.118(7) \text{ \AA}$ ,  $b = 7.733(9) \text{ \AA}$ ,  $c = 7.582(4) \text{ \AA}$ , Cmc $m$ ) in agreement with the JCPDF file 38-1418 (Table 1). Such oxides can also be synthesized using a conventional ceramic route by heating a mixture of  $R_2O_3$  and  $Ta_2O_5$  (or  $Nb_2O_5$ ) oxides at much higher temperatures ( $> 1350^\circ\text{C}$ ) [3,4]. However, the interpretation of the crystal structure appears to be confusing between authors. In the diffraction pattern of  $Gd_3TaO_7$  prepared by a polymerized complex method Abe et al. underlined the presence of several superlattice lines at 1350°C that prove the formation of a cubic pyrochlore structure, while Cai and Yokogawa indicate the formation of a weberite structure [3-8]. Under our experimental conditions using the citrate route and low temperatures, we have only observed the fluorite-type structure without any superlattice lines. The discrepancies about the  $R_3TaO_7$  structures comes mainly from the preparation route or the reaction temperature. All the structures are related to the fluorite-type. The use of *chimie douce* routes involves often the formation of metastable phases, leading to a competition between such phases and thermodynamically stable structures. The corresponding formulas  $R_3TaO_7$  and  $R_3NbO_7$  were confirmed by EDS and Leco<sup>®</sup> analyses (Table 1 and 2). Experimental oxygen contents are in good agreement with the calculated values. For example, in the case of  $Gd_3TaO_7$ , the experimental oxygen amount ( $14.9 \pm 0.1 \text{ wt.}\%$ ) matches well with the

calculated one (14.65 wt.%). All the samples are colorless except the holmium containing product for which the pale yellow results from 4f-4f transitions.

XRD patterns observed for  $R_3NbO_7$  are close to those of  $R_3TaO_7$  (Fig. 2a), evidencing a slight difference in the lattice parameters (Tables 1 and 2).  $R_3NbO_7$  phases with  $R = Eu, Gd, Ho, Y, Yb$  present a defect fluorite structure. The values of the cubic unit cell parameter decrease from europium to ytterbium and follow a linear relation. All  $R_3TaO_7$  and  $R_3NbO_7$  oxides were used in their X-ray amorphous state as precursors for nitridation. Similarly to the tantalum based compositions,  $R_3NbO_7$  powders are colorless (except for holmium).

### 3.2. $R_3(Ta/Nb)(O,N,\square)_8$ oxynitrides

The characteristics of the nitrated phases are given in Tables 3 and 4 for Ta- and Nb-based samples. The thermal reaction of the  $R_3TaO_7$  oxide precursors for the larger rare-earth elements  $R = La$  and  $Eu$  leads to a mixture of  $La_2O_3$  and  $LaTaON_2$  perovskite and a mixture  $Eu_3TaO_7$  (defect fluorite) +  $EuTa(O,N)_3$  (perovskite) respectively. It has not been possible to prepare an oxynitride single phase for these elements which may be attributed to the size of the involved lanthanides.  $La^{3+}$  ions are too large to fit in the 8-fold coordinated sites available in the  $R_3TaO_7$  fluorite-type structure and therefore occupy the 12-fold coordinated site in the perovskite structure. By comparison the case of  $Eu^{3+}$  is different.  $Eu^{3+}$  has a similar ionic radius than  $Gd^{3+}$  but under the reducing synthesis conditions,  $Eu^{3+}$  is reduced to  $Eu^{2+}$  which leads to the formation of the  $EuTa(O,N)_3$  [27].

In the case of gadolinium, the X-ray diffraction pattern indicates the formation of a fluorite-type phase (Fig. 1b). Using the experimental nitrogen content (1.00 wt.%)

and the electroneutrality of the formula, we have calculated the resulting defect fluorite composition  $\text{Gd}_3\text{TaO}_{5.67}\text{N}_{0.88}\square_{1.45}$  for the sample nitrated at  $950^\circ\text{C}$  during 15h (Table 3). A heating at higher temperature ( $1100^\circ\text{C}$ ) under  $\text{NH}_3$  leads to a black mixture composed of the nitride phase,  $\text{Ta}_2\text{O}_5$  and  $\text{Gd}_2\text{O}_3$  (Fig. 1c). As indicated in Table 5, the corresponding position of the absorption edge is located in the UV range of the spectrum ( $\lambda = 323$  nm, bandgap = 3.71 eV) resulting in a colorless powder (Fig. 3). Thus, the insertion of nitrogen in such a phase is not sufficient to generate an absorption in the visible. In order to shift the absorption edge towards larger wavelengths, we have totally substituted tantalum by niobium which has a higher electronegativity. It results a gadolinium-based oxynitride fluorite that is obtained at lower temperature ( $850^\circ\text{C}$ ) compared to the case of tantalum (Fig. 2b). A reaction over  $900^\circ\text{C}$  evidenced the formation of  $\text{Nb}(\text{O},\text{N})$  secondary phase (Fig. 2c). As expected, the ensuing diffuse reflectance study indicates an absorption edge shifted to 440 nm for  $\text{Gd}_3\text{NbO}_{6.17}\text{N}_{0.56}\square_{1.27}$  (Fig. 3). The higher covalency of the Nb-based phase explains the larger shift of the absorption edge when nitrated, compared to the tantalum one. For isostructural compounds the band gap decreases as the effective electronegativity of the transition metal ion increases [28]. From the spectrum profile of  $\text{Gd}_3\text{NbO}_{6.17}\text{N}_{0.56}\square_{1.27}$  are derived the color coordinates  $L = 83$ ,  $a^* = 1$ ,  $b^* = 16$  that are typical of the observed pale yellow color. Corresponding  $\text{Gd}_3\text{Nb}$ - and  $\text{Gd}_3\text{Ta}$ -based oxynitride phases have close lattice parameters, in relation with similar  $\text{Ta}^{5+}$  and  $\text{Nb}^{5+}$  ionic radii in 6-fold (0.64 Å) and 8-fold (0.74 Å) coordinated sites [21]. We observe the possibility to prepare an oxynitride fluorite phase with europium at  $700^\circ\text{C}$  which was not possible under our conditions with the analog tantalum composition (Table 4).

The R/Ta ratio influences also the characteristics of the series  $R_x\text{Ta-O-N}$ . The phases prepared and listed in Table 5 present a fluorite symmetry, except for the ratio  $\text{Gd/Ta}=1$  where an orange powder of the perovskite structure can be isolated at high temperature [1]. No evidence of low intensity extra peaks was pointed out as a sign of structural modification of the pyrochlore type for example. We observe increasing cubic parameters from the  $\text{RTa}$  to the  $\text{R}_3\text{Ta}$  oxynitride stoichiometries due to an increase of the radius of the average cation. When comparing the characteristics within the  $\text{Gd}_x\text{Ta-O-N}$  series, a shift of the absorption edge towards UV is observed on the diffuse reflectance spectrum with increasing Gd/Ta ratio in parallel with a change in color from yellow to white (Fig. 4). The study has been extended in a similar approach to compositions with different Gd/Nb ratios in order to evaluate the effect of the substitution on the color. Unfortunately, the nitridation of the amorphous oxide  $\text{GdNbO}_4$  prepared by the citrate route leads to a mixture  $\text{Gd}_2\text{O}_3 + \text{Nb(O,N)}$ . Although no oxide phase was reported with the stoichiometry  $\text{Gd}_2\text{NbO}_{5.5}$ , the ammonolysis of this amorphous phase between  $700^\circ\text{C}$  and  $900^\circ\text{C}$  produces a grey oxynitride powder with a fluorite structure, whereas at  $1000^\circ\text{C}$ , a mixture  $\text{Gd}_2\text{O}_3 + \text{Nb(O,N)}$  is formed. These stoichiometries are thus not intended for suitable optical properties.

With the smaller rare earth elements  $R = \text{Ho, Y, Yb}$ , novel Ta and Nb-based oxynitride phases have been isolated with a defect fluorite structure (Tables 3 and 4). Corresponding lattice parameters follow a linear relation and decrease from gadolinium to ytterbium as expected (Fig. 5). Compared to the corresponding oxide precursors (Tables 1 and 2), Ta and Nb-based oxynitrides show higher parameter values due to the insertion of nitrogen (Tables 3 and 4). In the case of Yb, both tantalum-based oxide and

oxynitride parameters are very close. As indicated in Tables 3 and 4, the powders are generally little colored with a poor brightness. Similarly to the case of gadolinium, when modifying the ratio from RTa to R<sub>2</sub>Ta and R<sub>3</sub>Ta ratios, the oxynitride unit cell parameter increases, for example, respectively from 5.201(1) to 5.229(1) and 5.244(3) Å for Y and from 5.100(1) to 5.159(1) and 5.167(2) Å for Yb [1-2]. In comparison with RTa and R<sub>2</sub>Ta samples, colored R<sub>3</sub>Ta- and R<sub>3</sub>Nb- oxynitrides manifest a limited thermal stability range of approximately 50°C around the reaction temperatures (T) given in Table 3 and 4. The increase of the reaction step to 3 cycles of 15 hours gives rise to a limited panel of nitrogen contents within the oxynitride compositions (Tables 6 and 7). The fluorite structure manifests enough flexibility in general to form domains of solid solutions, quite restricted in our case, at 950°C for Ta compositions and from 700 to 850°C for Nb samples. Compared to the ratio Gd/Ta = 1 [1], we observe with increasing nitridation time a decrease of the nitrogen content. We suppose that R<sub>3</sub>Ta or R<sub>3</sub>Nb-oxynitrides present a shorter range of stability compared to that of RTa or RNb compounds. A competition between nitrogen enrichment and decomposition may occur. Heatings performed over 950°C lead quite rapidly to dark powders, attesting of a partial reduction of the transition metal.

#### **4. Conclusion**

We have shown the possibility to insert nitrogen within R<sub>3</sub>Ta-O and R<sub>3</sub>Nb-O systems leading to fluorite-type oxynitrides. The panel of resulting colors do not lead to bright hues in comparison with previous work in the RTa stoichiometry. A blue shift of the absorption is clearly observed when increasing the R/Ta ratio. In order to modify the

colors of the oxynitrides, tantalum atoms were substituted by niobium atoms in the  $Gd_3TaO_7$  precursor where a significant change of coloration is observed as a consequence of the shift of the absorption edge towards visible radiations. Solid solution domains obtained from R=Gd to Yb in the  $R_3Ta$  and  $R_3Nb$  stoichiometries evidence a limited range of stability.

## References

- [1] P. Maillard, F. Tessier, E. Orhan, F. Chevire and R. Marchand, *Chem. Mater.* 17 (2005) 152-156.
- [2] P. Maillard, O. Merdrignac-Conanec and F. Tessier, *Mater. Res. Bull.* 43 (2008) 30-37.
- [3] Y. Yokogawa, M. Yoshimura and S. Somiya, *Solid State Ion.* 35 (1989) 275-279.
- [4] Y. Yokogawa, M. Yoshimura and S. Smiya, *Solid State Ion.* 28-30 (1988) 1250-1253.
- [5] Y. Yokogawa, M. Yoshimura and S. Somiya, *Mater. Res. Bull.* 22 (1987) 1449-1456.
- [6] R. Abe, M. Higashi, Z. Zou, K. Sayama, Y. Abe and H. Arakawa, *J. Phys. Chem. B.* 108 (2004) 811-814.
- [7] R. Abe, M. Higashi, K. Sayama, Y. Abe and H. Sugihara, *J. Phys. Chem. B.* 110 (2006) 2219-2226.
- [8] L. Cai and J. C. Nino, *J. Eur. Ceram. Soc.* 27 (2007) 3971-3976.
- [9] F. Cheviré, F. Tessier and R. Marchand, *Eur. J. Inorg Chem.* (2006) 1223-1230.
- [10] M. Jansen, H.P. Letschert *Nature* 404 (2000) 980-982.
- [11] F. Tessier and R. Marchand, *J. Solid State Chem.* 171 (2003) 143-151.
- [12] F. Tessier, P. Maillard, F. Cheviré, K. Domen and S. Kikkawa, *J. Ceram. Soc. Jpn* 117 (2009) 1-5.
- [13] R. Aguiar, D. Logvinovich, A. Weidenkaff, A. Rachel, A. Reller, S.G. Ebbinghaus, *Dye and Pigments* 76 (2008) 70-75

- [14] R. Xie, N. Hirosaki, *Sci. Technol. Adv. Mat.* 8 (2000) 588-600
- [15] A. Fuertes, *Dalton Trans.* 39 (2010) 5942-5948
- [16] R. Asahi, T. Morikawa, T. Ohwaki, K. Aoki and Y. Taga, *Science* (1998), 425-427.
- [17] M. Gohin, I. Maurin, T. Gacoin, J.P. Boilot, *J. mater. Chem.* 20 (2010), 8070-8077.
- [18] K. Maeda and K. Domen, *Chem. Mater.* 22 (2009) 612-623.
- [19] K. Maeda and K. Domen, *J. Phys. Chem. C.* 111 (2007) 7851-7861.
- [20] M. Yoshida, T. Hirai, K. Maeda, N. Saito, J. Kubota, H. Kobayashi, Y. Inoue, K. Domen, *J. Phys. Chem. C* 114 (2010) 15510-15515.
- [21] A. Douy and P. Odier, *Mater. Res. Bull.* 24 (1989) 1119-1126.
- [22] A. Boultif and D. Louer, *J. Appl. Crystallogr.* 24 (1991) 987-993.
- [23] M. Dopita, B. Wollein, D. Rafaja, W. Gruner and W. Lengauer, *Defect and Diffusion Forum, Diffusion in Materials DIMAT-2000.* 194-199 (2001) 1613-1618.
- [24] D. Kubelka, L. Munk and Z. Teck, *Phys.* 12 (1931) 987-993.
- [25] ICDD- Powder diffraction files PDF-2 database set 1-49.
- [26] F. Chevire, F. Clabau, O. Larcher, E. Orhan, F. Tessier and R. Marchand, *Solid State Sci.* 11 (2009) 533-536
- [27] R.D. Shannon, *Acta Cryst.* A32 (1976) 751-767
- [28] H. W. Eng, P. W. Barnes, B. M. Auer, P. M. Woodward, *J. Solid State Chem*, 2003, 175, 94-109.

**Table 1**Experimental characteristics of  $R_3TaO_7$  phases prepared at 1000°C.

<b>Element</b>	<b>XRD</b>	<b>Lattice parameters (Å)</b>	<b>O wt.% (experimental)</b>	<b>O wt.% (calculated)</b>	<b>Color</b>
La	weberite	a = 11.118(7) b = 7.733(9) c = 7.582(4)	16.1	15.78	white
Eu	fluorite	5.319(3)	14.5	14.96	white
Gd	fluorite	5.307(3)	14.9	14.65	white
Ho	fluorite	5.223(4)	14.3	14.22	pale yellow
Y	fluorite	5.220(7)	19.9	20.01	white
Yb	fluorite	5.170(4)	14.1	13.79	white

**Table 2**Experimental characteristics of  $R_3NbO_7$  phases prepared at 1000°C.

<b>Element</b>	<b>XRD</b>	<b>Lattice parameter (Å)</b>	<b>O wt.% (experimental)</b>	<b>O wt.% (calculated)</b>	<b>color</b>
Eu	fluorite	5.325(2)	16.7	16.95	white
Gd	fluorite	5.305(3)	16.4	16.55	white
Ho	fluorite	5.229(3)	16.3	16.01	pale yellow
Y	fluorite	5.241(2)	23.1	23.75	white
Yb	fluorite	5.191(2)	15.7	15.47	white

**Table 3**Experimental characteristics of nitrated  $R_3TaO_7$  phases (950°C - 15h).

<b>Element</b>	<b>XRD</b>	<b>Lattice parameter (Å)</b>	<b>N wt.% (experimental)</b>	<b>Formula</b>	<b>Color</b>
La	$La_2O_3 + LaTaON_2$	-	-	-	orange
Eu	$Eu_3TaO_7 + EuTa(O,N)_3$	-	0.95	-	beige
Gd	defect fluorite	5.317(2)	1.64	$Gd_3TaO_{5.67}N_{0.88}\square_{1.45}$	white
Ho	defect fluorite	5.252(1)	1.32	$Ho_3TaO_{5.90}N_{0.73}\square_{1.37}$	pale yellow
Y	defect fluorite	5.244(3)	1.74	$Y_3TaO_{5.97}N_{0.69}\square_{1.34}$	whitish
Yb	defect fluorite	5.167(2)	1.62	$Yb_3TaO_{5.61}N_{0.93}\square_{1.46}$	beige

**Table 4**Experimental characteristics of nitrided of  $R_3NbO_7$  phases (reaction step = 15h).

<b>Element</b>	<b>XRD</b>	<b>Nitridation temperature (°C)</b>	<b>Lattice parameter (Å)</b>	<b>N wt.% (experimental)</b>	<b>Formula</b>	<b>Color</b>
Eu	defect fluorite	700	5.331(2)	0.47	$Eu_3NbO_{6.67}N_{0.22}\square_{1.11}$	white
Gd	defect fluorite	850	5.316(2)	1.16	$Gd_3NbO_{6.17}N_{0.56}\square_{1.27}$	pale yellow
Ho	defect fluorite	700	5.248(2)	0.88	$Ho_3NbO_{6.34}N_{0.44}\square_{1.22}$	pale yellow
Y	defect fluorite	750	5.265(1)	1.88	$Y_3NbO_{6.06}N_{0.62}\square_{1.32}$	white
Yb	defect fluorite	700	5.194(1)	1.01	$Yb_3NbO_{6.22}N_{0.52}\square_{1.26}$	pale yellow

**Table 5**

Characteristic values from the diffuse reflectance spectra of the Gd<sub>x</sub>Ta-O-N samples series.

<b>Composition</b>	<b>Gd/Ta</b>	<b>Lattice parameter (Å)</b>	<b><math>\lambda \pm \Delta\lambda</math> (nm)</b>	<b>E<sub>g</sub> (eV)</b>	<b>color</b>
GdTaO <sub>2.33</sub> N <sub>1.12</sub> O <sub>0.55</sub>	1	5.205(2)	553 ± 70	2.58	yellow
GdTaON <sub>2</sub>	1	$a = 5.552(3)$ $b = 5.690(2)$ $c = 7.923(3)$	561 ± 31	2.21	orange
Gd <sub>2.4</sub> Ta <sub>1.6</sub> O <sub>3.26</sub> N <sub>2.89</sub> O <sub>1.85</sub>	1.5	5.246(2)	428 ± 65	2.75	pale yellow
Gd <sub>2.67</sub> Ta <sub>1.33</sub> O <sub>5.53</sub> N <sub>1.20</sub> O <sub>1.27</sub>	2	5.271(4)	389 ± 55	3.04	pale yellow
Gd <sub>2.86</sub> Ta <sub>1.14</sub> O <sub>6.16</sub> N <sub>0.65</sub> O <sub>1.19</sub>	2.5	5.298(3)	337 ± 27	3.61	whitish
Gd <sub>3</sub> TaO <sub>5.67</sub> N <sub>0.88</sub> O <sub>1.45</sub>	3	5.317(2)	323 ± 26	3.71	whitish

**Table 6** $R_3Ta(O,N,\square)_8$  fluorite-type solid solutions: composition and color.

<b>R</b>	<b>Thermal ammonolysis conditions</b>	<b>N wt. %</b>	<b>Experimental formulation</b>	<b>Color</b>
Gd	5 h, 950°C	1.81	$Gd_3TaO_{5.54}N_{0.98}\square_{1.48}$	white
	15 h, 950°C	1.64	$Gd_3TaO_{5.67}N_{0.88}\square_{1.45}$	
Ho	15h, 950°C	1.32	$Ho_3TaO_{5.90}N_{0.73}\square_{1.37}$	pale yellow
	2 x 15h, 950°C	1.27	$Ho_3TaO_{5.94}N_{0.71}\square_{1.35}$	
Y	15h, 950°C	1.74	$Y_3TaO_{5.97}N_{0.69}\square_{1.34}$	whitish
	3 x 15h, 950°C	1.63	$Y_3TaO_{6.03}N_{0.64}\square_{1.33}$	
Yb	15h, 950°C	1.62	$Yb_3TaO_{5.61}N_{0.93}\square_{1.46}$	beige
	2 x 15h, 950°C	1.53	$Yb_3TaO_{5.68}N_{0.88}\square_{1.44}$	

**Table 7**

$R_3Nb(O,N,\square)_8$  fluorite-type solid solutions: composition and color.

<b>R</b>	<b>Thermal ammonolysis</b>	<b>N wt. %</b>	<b>Experimental formulation</b>	<b>Color</b>
Eu	15h, 700°C	0.47	$Eu_3NbO_{6.67}N_{0.22}\square_{1.11}$	white
	3 x 15h, 700°C	0.44	$Eu_3NbO_{6.69}N_{0.21}\square_{1.10}$	
Gd	15h, 850°C	1.16	$Gd_3NbO_{6.17}N_{0.56}\square_{1.27}$	pale yellow
	2 x 15h, 850°C	1.23	$Gd_3NbO_{6.12}N_{0.59}\square_{1.29}$	
Ho	15h, 700°C	0.88	$Ho_3NbO_{6.34}N_{0.44}\square_{1.22}$	pale yellow
	3 x 15h, 700°C	0.86	$Ho_3NbO_{6.36}N_{0.43}\square_{1.21}$	
Y	15h, 750°C	1.88	$Y_3NbO_{6.06}N_{0.62}\square_{1.32}$	white
	2 x 15h, 750°C	1.77	$Y_3NbO_{6.12}N_{0.59}\square_{1.29}$	
Yb	15h, 700°C	1.01	$Yb_3NbO_{6.22}N_{0.52}\square_{1.26}$	pale yellow
	3 x 15h, 700°C	0.87	$Yb_3NbO_{6.33}N_{0.45}\square_{1.22}$	

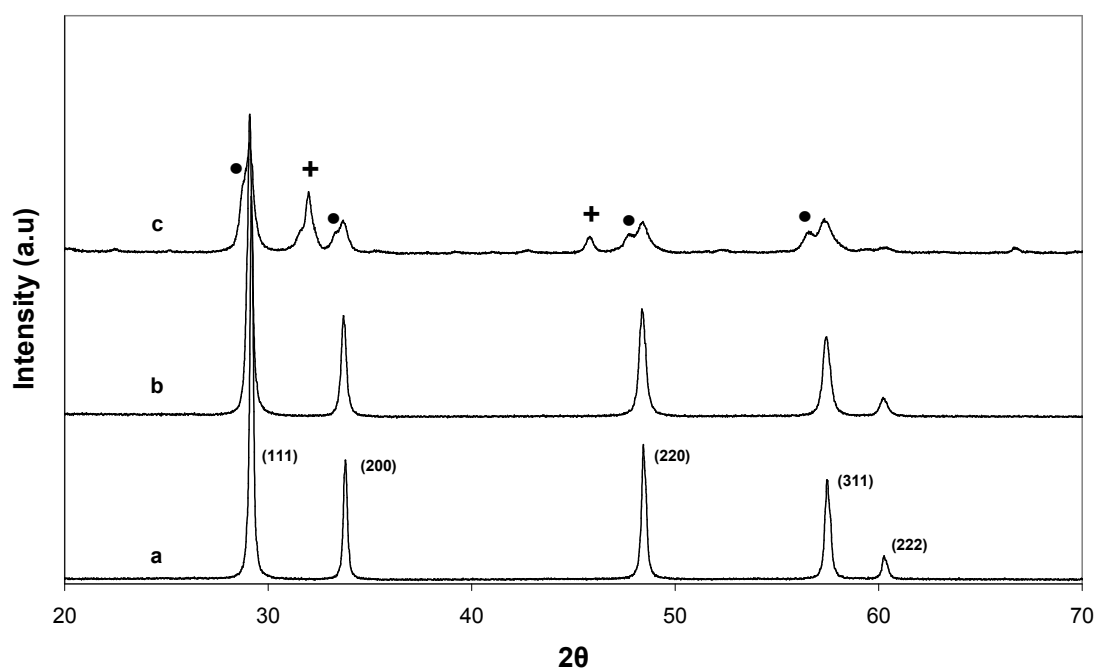


**Fig. 1.** XRD powder pattern of  $Gd_3TaO_7$  prepared at  $1000^\circ C$  (a),  $Gd_3TaO_7$  nitrided at  $950^\circ C/15h$  (b) corresponding to  $Gd_3TaO_{5.67}N_{0.88}O_{1.45}$  and  $Gd_3TaO_7$  nitrided at  $1100^\circ C/15h$  (c) leading to a mixture including  $Gd_2O_3$  (•) and  $Ta_2O_5$  (+).

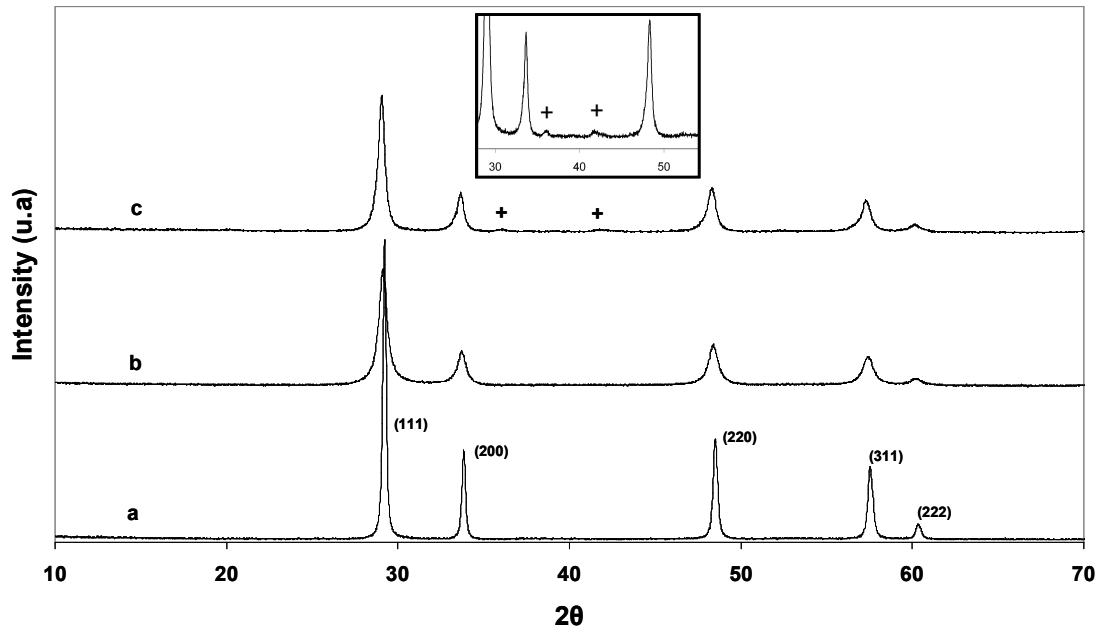


**Fig. 2.** XRD powder pattern of  $\text{Gd}_3\text{NbO}_7$  prepared at  $1000^\circ\text{C}$  (a),  $\text{Gd}_3\text{NbO}_7$  nitrified at  $850^\circ\text{C}/15\text{h}$  (b) and  $\text{Gd}_3\text{NbO}_7$  nitrified at  $900^\circ\text{C}/15\text{h}$  (c) with the formation of  $\text{Nb}(\text{O},\text{N})$  (+).

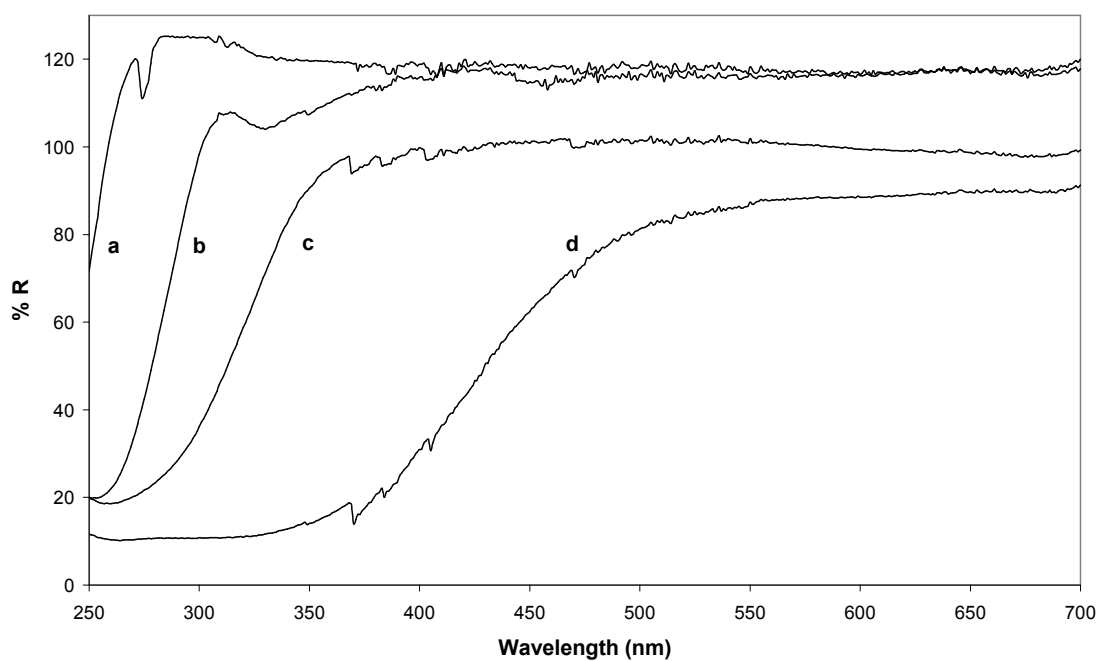


**Fig 3.** Diffuse reflectance spectra of the oxides  $\text{Gd}_3\text{TaO}_7$  (a),  $\text{Gd}_3\text{NbO}_7$  (b) and the corresponding oxynitrides  $\text{Gd}_3\text{TaO}_{5.67}\text{N}_{0.88}\square_{1.45}$  (c) and  $\text{Gd}_3\text{NbO}_{6.17}\text{N}_{0.56}\square_{1.27}$  (d).

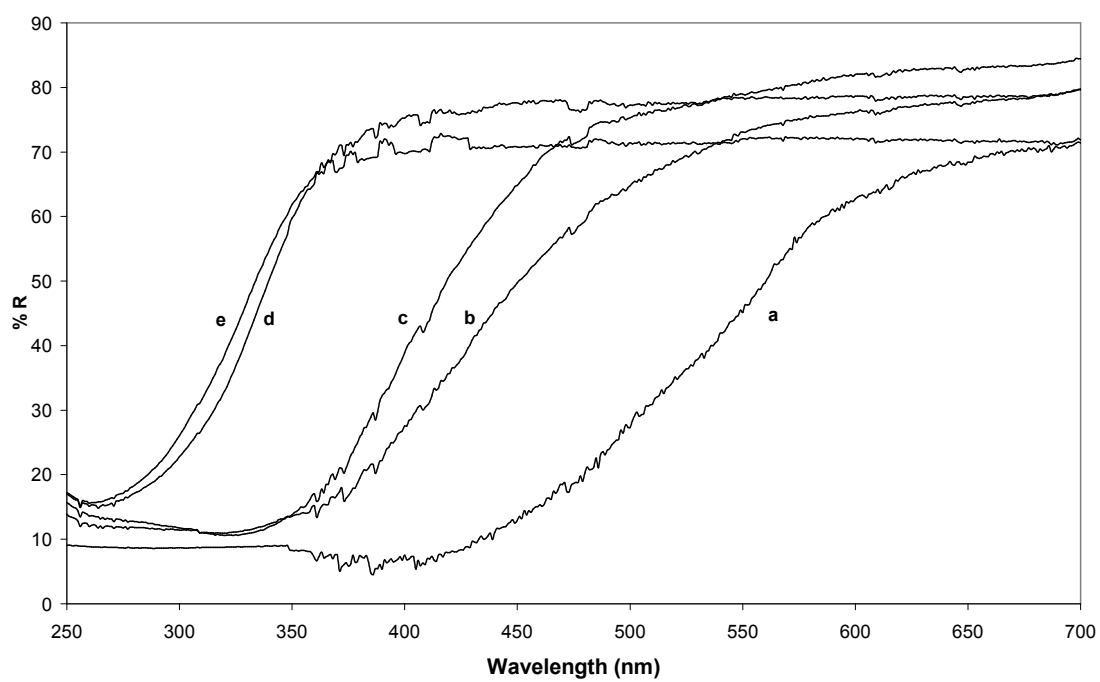


**Fig 4.** Diffuse reflectance spectra of the oxynitrides:  $\text{GdTaO}_{2.33}\text{N}_{1.12}\square_{0.55}$  (a),  $\text{Gd}_{2.4}\text{Ta}_{1.6}\text{O}_{3.26}\text{N}_{2.89}\square_{1.85}$  (b),  $\text{Gd}_{2.67}\text{Ta}_{1.33}\text{O}_{5.53}\text{N}_{1.20}\square_{1.27}$  (c),  $\text{Gd}_{2.86}\text{Ta}_{1.14}\text{O}_{6.16}\text{N}_{0.65}\square_{1.19}$  (d),  $\text{Gd}_3\text{TaO}_{5.67}\text{N}_{0.88}\square_{1.45}$  (e).

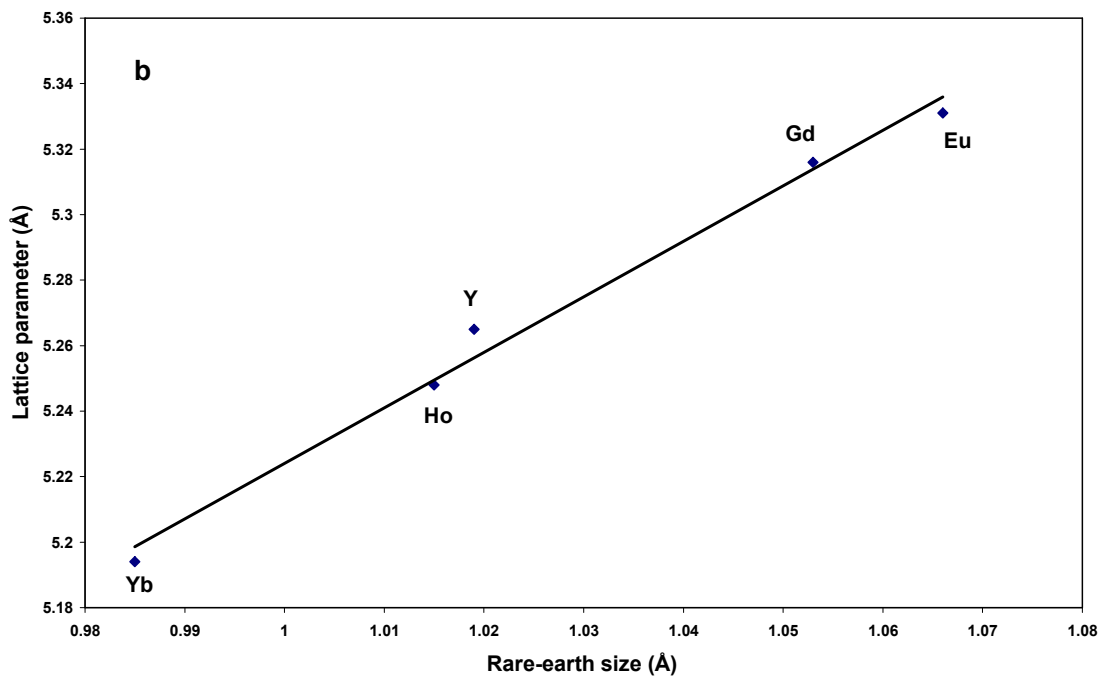
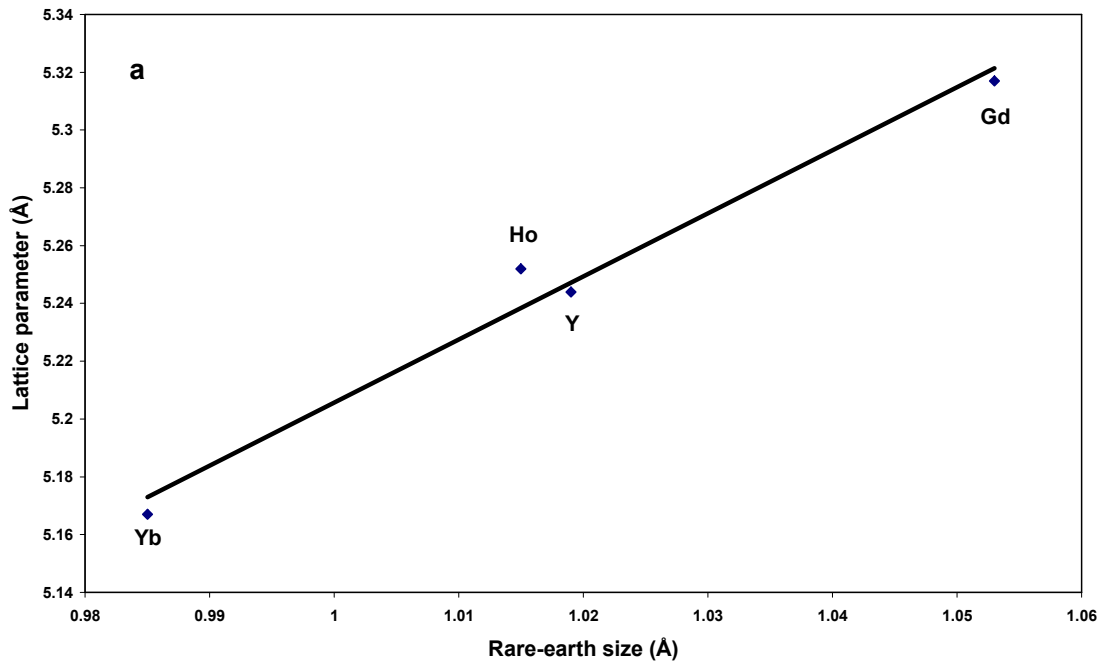


**Fig. 5.** Evolution of the lattice parameter with the rare-earth ionic radius in the tantalum (a) and niobium(b) cases.